Nano Energy 23 (2016) 70–79

Contents lists available at ScienceDirect

Nano Energy

journal homepage: www.elsevier.com/locate/nanoen

Extremely stable bare hematite photoanode for solar water splitting

Paula Dias [1], António Vilanova [1], Tânia Lopes, Luísa Andrade, Adélio Mendes *

LEPABE – Faculdade de Engenharia, Universidade do Porto, rua Dr. Roberto Frias, 4200-465 Porto, Portugal

ARTICLE INFO

Article history:
Received 28 December 2015
Received in revised form
4 March 2016
Accepted 9 March 2016
Available online 10 March 2016

Keywords:
Hematite photoanodes
Photoelectrochemical water splitting
Spray pyrolysis
Design of experiments
Thin films
Long-term stability

ABSTRACT

Photoelectrodes that are efficient, highly stable, made from low cost materials and easily prepared using inexpensive techniques are required for commercially viable solar photoelectrochemical (PEC) water-splitting technology. Hematite is one of few materials that is being considered for this application. In this work, bare hematite thin films prepared by spray pyrolysis were systematically optimized following a design of experiments approach. A response surface methodology was applied to factors: (i) sprayed volume of solution; (ii) temperature of the glass substrate during the deposition; and (iii) time gap between sprays and the optimized operating conditions obtained were $v=42$ mL, $T=425$ °C and $t=35$ s. The optimized hematite photoelectrode showed a photocurrent density of *ca.* 0.94 mA cm^{-2} at 1.45 V_{RHE}, without dopants or co-catalysts, which is remarkable for a thin film of *ca.* 19 nm. The stability of this photoelectrode was assessed over 1000 h of PEC operation under 1-sun of simulated sunlight. A record-breaking result was obtained with no evidences of hematite film degradation neither of current density loss. These results open the door to turn PEC cells into a competitive technology in the solar fuel economy.

© 2016 Published by Elsevier Ltd.

1. Introduction

Due to the world increasing of population and industrialization the total power consumption is expected to increase up to 30 TW by 2050; fossil fuels, which currently provide about 85% of mankind energy supply, will be unable to keep up this demand [1,2]. Moreover, in the last few years the consumption of fossil fuels never stopped growing and this behavior is projected for the next decades [3]. As side effects, global warming consequences, natural resources depletion and global health deterioration are expected to be gradually intensified. Thus, it is crucial to develop alternative and environmentally friendly technologies to efficiently harvest energy from renewable sources [4]. Solar energy is believed to be a potential solution for sustainable energy use, since it can realistically be implemented on a large scale to supply the current world energy demand [5]. However, concerning to the intermittent nature of solar irradiance, technologies that convert sunlight into storable forms of energy, namely into fuels, are needed. Hydrogen has been considered a sustainable green fuel for the future when used as feedstock of fuel cells [6]. Therefore, the efficient solar photoelectrochemical (PEC) water splitting to produce storable hydrogen is a critical research area [7,8].

A typical PEC cell consists of a light-absorbing photoelectrode and a counter-electrode immersed in an aqueous electrolyte solution. The main component of a PEC device is the semiconductor, which converts incident photons to electron–hole pairs when exposed to sunlight. The key requirements for a semiconductor photoelectrode are: (i) efficient absorption of visible light; (ii) suitable band edge positions for hydrogen and oxygen evolutions; (iii) high photopotential efficiency; (iv) good charge transport; (v) low kinetic overpotentials; and (vi) high stability in aqueous electrolyte solutions [9]. Considering an n-type semiconductor, holes exhibit oxidation potential while the electrons are transferred over the external circuit to the counter-electrode (cathode) to promote the water reduction into hydrogen. In alkaline medium, water reduction ions generated at the cathode, OH^-, diffuse back to the semiconductor surface (photoanode) to react with holes and produce oxygen [10].

In 1972, Fujishima and Honda were the first authors to report the splitting of water in a PEC cell using a TiO_2 photoanode under UV light [11]. Since then, many research efforts have been made to find a suitable material for preparing stable and high-performance photoelectrodes [12,13]. Numerous metal oxide semiconductors have been tested for PEC photoanodes and hematite (α-Fe_2O_3) is emerging as one of the most promising materials [12,13]. Hematite offers a favorable combination of good visible light absorption (up to 590 nm), excellent chemical stability, non-toxicity, abundance and low price [15,16]. Additionally, with a small band gap of *ca.* 2.1 eV, it can reach a high thermodynamic solar-to-hydrogen (STH) conversion efficiency of 14–17%, which corresponds to a photocurrent generation of 11–14 mA cm^{-2} under standard air mass

* Corresponding author.
E-mail address: mendes@fe.up.pt (A. Mendes).
[1] These authors contributed equally.

http://dx.doi.org/10.1016/j.nanoen.2016.03.008
2211-2855/© 2016 Published by Elsevier Ltd.

(AM) 1.5 G illumination (100 mW cm^{-2}) [12,14]. Nevertheless, while its valence band is well positioned to oxidize water, the conduction band is too low for water reduction to hydrogen and so a bias has to be applied to accomplish water splitting. Since the ideal PEC system should work without an external bias, a combination of two or more semiconductors, *e.g.* a photocathode [15] or a photovoltaic (PV) cell [16,17] in a tandem arrangement, would overcome this drawback. Despite all these advantages, the high rate of electron–hole recombination and the short hole diffusion length of hematite (2–4 nm) are the major factors limiting the STH efficiency [18].

The first study on hematite ability for water photolysis was published in 1976 by Hardee and Bard [19]. These authors found hematite to be highly stable in neutral and alkaline electrolytes solutions. Presently, the main ongoing studies on hematite concern: (i) improvement of generated photocurrent density by morphology optimization and doping; (ii) improvement of generated photopotential minimizing the hole–electron recombination, especially at the photoelectrode surface; and (iii) reduction of the electrochemical activation overpotential using, *e.g.* co-catalysts [20,21]. However, stability/long-term performance of the photoelectrode is also of critical importance. Most reports assess lifetime of semiconductors during less than 24 h. Only few semiconductor-liquid junction (SCLJ) devices demonstrated to display stabilities of more than 1 day [22].

The performance of hematite photoanodes is very sensitive to the deposition method, either in terms of efficiency and stability. Innovative ways to control the morphology should be developed to optimize the hematite feature size/film thickness and crystals structure at nanometer length scale [23]. There are many deposition methods reported to deposit hematite: (i) solution-based colloidal [24]; (ii) electrochemical iron oxide nanostructuring; (iii) spray pyrolysis [25]; (iv) atmospheric pressure chemical vapor deposition (APCVD) [26]; (v) physical vapor deposition (PVD) [27]; and (vi) atomic layer deposition (ALD) [18]. Table S1 (available in the Supplementary material – SM) reviews the hematite photoanodes literature, indicating the preparation techniques and the obtained photoresponse and stability. Recently, Tan et al. [28] reported a new record-breaking of *ca.* 5.70 mA cm^{-2} at 1.23 V_{RHE} with Ru-doped α-Fe_2O_3 nanorods films. This highly photoactive material was prepared by deposition of the [Ru(acac)$_3$]-treated presynthesized ultrathin α-FeOOH nanorods precursors onto FTO substrates via a doctor blading process and followed by annealing at 700 °C in air, showing a film thickness of 500 nm. However, the preparation of hematite thin films is desirable considering their charge transport limitation, *i.e.* thin films should minimize the recombination losses while light absorption is adaptable by the nanostructure thickness. Indeed, spray pyrolysis and ALD are the techniques that allow to deposit thinner films with good uniformity and photocurrent performance.

In the present study, hematite thin films were prepared by spray pyrolysis exhibiting high performance and great reproducibility, which is crucial for future industrial applications. The prepared hematite thin films revealed to be highly stable producing *ca.* 0.94 mA cm^{-2} at 1.45 V_{RHE} over 1000 h of sunlight exposure (AM 1.5 G, 100 mW cm^{-2}) in a 1.0 M NaOH electrolyte solution.

2. Experimental section

2.1. Hematite photoanodes preparation

The synthesized materials were prepared by spray pyrolysis in an in-house assembled setup consisting of: (i) spray pyrolysis chamber; (ii) automatic syringe pump; (iii) liquid and air feeding system; (iv) spray nozzle and its control system; (v) heating plate and its control system – Fig. 1. The spray nozzle (Spraying Systems Co. model SU J4B-SS) was fed with an ethanolic solution of iron (iron (III) acetylacetonate – Fe(AcAc)$_3$) and mixed with compressed air, directing the spray to the substrates at *ca.* 2 bar. An automatic syringe pump (Cronus programmable Sigma 2000 C, SMI-Labhut Ltd., UK) was used to deliver 1 mL of 10 mM of Fe(AcAc)$_3$ (99.9%, Aldrich) in EtOH (99.5%, Aga) to the spray head, at a flowrate of 12 mL min^{-1} (spray length of 5 s). The heated plate, 18 × 18 cm^2, displayed a uniform surface temperature regulated up to 550 °C. The substrates were placed on the heated plate at constant temperature; a range of 400–500 °C was tested. After the spray deposition, the hematite samples were air-annealed for 30 min at 550 °C, before being cooled down to the room temperature. This setup allows depositing homogeneous films up to 10 × 10 cm^2. For each set of parameters tested, three samples were prepared to assess the reproducibility.

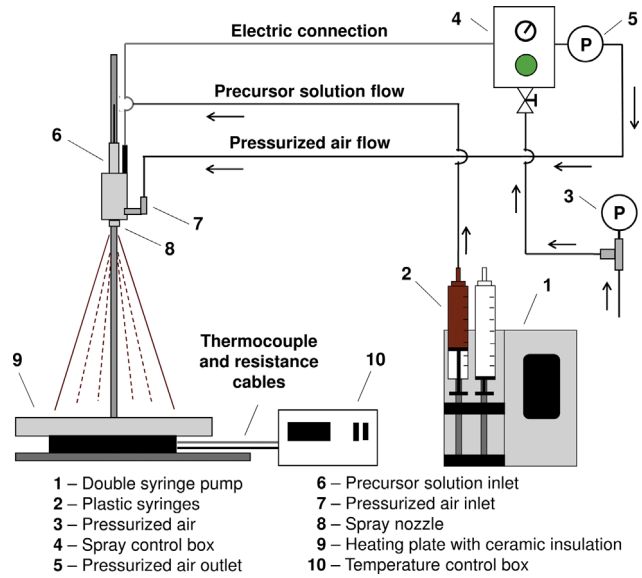

Fig. 1. Schematic representation of the spray pyrolysis setup for hematite deposition.

The photoanodes were prepared on 2.2 mm thick, 7 Ω square^{-1} fluorine-doped tin oxide (FTO) coated glass substrates (Solaronix, Switzerland). The glasses were adequately cleaned as described elsewhere [29]. A TEOS (tetraethyl orthosilicate) pre-treatment was also performed to allow better Fe_2O_3 film organization, reducing the interfacial strain between the FTO layer and the hematite crystals and, consequently, a photoactivity response improvement [30]. The FTO-glass substrates were heated at 450 °C and *ca.* 1.5 mL of a diluted TEOS solution (10% volume in ethanol) were hand-sprayed with a glass atomizer onto the heated substrates. These samples were cooled down before heating again to deposit the hematite film.

2.2. Response surface methodology

According to literature [31,32], the deposition of hematite films by spray pyrolysis technique strongly depends on several operating parameters. An optimization procedure is necessary to obtain the best operating conditions and, therefore, to develop an efficient and stable photoanode. This optimization was done using a response surface methodology implemented in a commercial software (JMP 8.0.2, SAS software). This method combines mathematical and statistic tools for studying effective way processes where responses are dependent on several operating variables [33]. In this work the central composite design method was considered for fitting the obtained second order models. The selected

Table 1
Central composite design factors and their respective levels.

Factor	Symbol	Level		
		−1	0	1
v/mL	$x1$	30	45	60
T/°C	$x2$	400	450	500
t/s	$x3$	30	45	60

response variable was the photocurrent density (J, in mA cm^{-2}) generated by the prepared material at a bias potential of 1.45 V_{RHE}.

Several preliminary tests were performed to assess the influence of different operating conditions on the performance of the bare hematite photoanodes. The deposition parameters selected for optimization were: (i) sprayed solution volume (v); (ii) temperature of the glass substrate during the deposition (T); and (iii) time gap between sprays (t) – Table 1. The following parameters were set constant: (i) concentration of the iron solution was 10 mM; (ii) distance of the spray head to the sample was 20 cm and; (iii) annealing temperature was 550 °C.

For generating the design matrices, dimensionless (coded) factors (X_i), ranging from −1 to +1 were used. These factors are computed from their actual values (x_i), middle value and the semi-variation interval according to [34]:

$$X_1 = \frac{x_1 - 45}{15}; \quad X_2 = \frac{x_2 - 450}{50}; \quad X_3 = \frac{x_3 - 45}{15} \tag{1}$$

2.3. Electrochemical characterization

A PEC cell device known as "cappuccino" was chosen to perform the electrochemical characterization of the prepared hematite photoanodes [35]. This cell was filled with a 1.0 M NaOH (25 °C, pH = 13.6) electrolyte solution in which the photoelectrode was immersed. The surface area illuminated was *ca.* 0.5 cm^2 defined by an external mask. A standard three-electrode configuration was used: Ag/AgCl/Sat KCl electrode (Metrohm, Switzerland) used as a reference electrode, 99.9% pure platinum wire (Alfa Aesar®, Germany) as counter-electrode and hematite photoanodes as working electrodes.

2.3.1. Photocurrent–voltage (J–V) measurements

J–V characteristic curves were obtained applying an external potential bias to the cell and measuring the generated photocurrent using a ZENNIUM workstation (Zahner Elektrik, Germany) controlled by Thales software package (Thales Z 2.0). The applied potential bias was reported as a function of the reversible hydrogen electrode (RHE). The measurements were performed at room temperature in dark and under 1-sun simulated sunlight, at a scan rate of 10 mV s^{-1} between 0.8 and 1.8 V_{RHE}. A class B solar simulator equipped with a 150 W Xe lamp (Oriel, Newport, USA) and an AM 1.5 G filter (100 mW cm^{-2}; Newport, USA) was used and the light beam was calibrated with a c-Si photodiode (Newport, USA).

2.3.2. Electrochemical impedance spectroscopy (EIS) measurements

EIS analyses were performed applying a small potential sinusoidal perturbation to the system. The amplitude and the phase shift of the resulting current response was recorded using also the ZENNIUM workstation. The frequency range was 0.1 Hz to 100 kHz and the amplitude 10 mV. The measurements were carried out in dark conditions and the range of the applied potential was equal to that of the photocurrent measurements (0.8–1.8 V_{RHE}) with a step of 50 mV. An appropriate electrical analog was then fitted to the EIS spectra using the ZView software (Scribner Associates Inc., USA).

2.3.3. Stability measurements

During stability tests hematite photoanodes were continuously submitted to simulated solar irradiance (100 mW cm^{-2}, AM 1.5 G) at 1.45 V_{RHE}. The photocurrent density response was monitored as a function of time using an AUTOLAB electrochemical station (Metrohm Autolab B.V., Netherlands). The lamp power used was a Plasma-I AS1300 light engine (Plasma International, Germany) equipped with a standard sulfur lamp (SS0); a c-Si photodiode was used for calibration. The photocurrent history of the prepared hematite photoanodes was assessed over 1000 h.

2.4. Determination of intrinsic solar to chemical conversion efficiency

Rothschild et al. [36] proposed the intrinsic solar to chemical (*ISTC*) conversion efficiency model, obtained from the photocurrent density–voltage (J–V) characteristic curves in the dark and under illumination. Briefly, this parameter indicates the efficiency of the photoanode in converting photonic energy into chemical energy used for oxidizing water. Thus, the *ISTC* efficiency of the photoanode is given by [36]:

$$ISTC = \left[\eta_{el}\frac{J_{photo} \times V_{photo}}{P_{light}}\right]_{AM\ 1.5\ G} \cong \frac{1.23(V_{RHE})}{U_{dark}(V_{RHE})}\left[\frac{J_{photo}(mA{\cdot}cm^{-2}) \times V_{photo}(V)}{100(mW{\cdot}cm^{-2})}\right] \tag{2}$$

where η_{el} is the electrolysis efficiency, J_{photo} is the generated photocurrent, V_{photo} is the correspondent photopotential and U_{dark} is the potential that must be applied to the photoanode in order to reach the respective current in the dark [36]. After computing the photocurrent (J_{photo}) and photopotential (V_{photo}) from J–V curves, the photocurrent as a function of the photopotential was drawn to obtain the intrinsic photovoltaic characteristics of the photoanode. The intrinsic photovoltaic power (P) of the photoanode is the product of photocurrent to the photopotential; by plotting it versus photopotential, the maximum power point (MPP) can be obtained and also the respective potential (V_{MPP}) and current (J_{MPP}).

2.5. Structural characterization

2.5.1. Film thickness determination

UV–visible absorption data were used to estimate the hematite samples thickness. Since there is a similarity in the shape of the spectra for all samples, their thicknesses can be estimated assuming a Lambertian absorption behavior:

$$\ln(1 - A) = -\alpha{\cdot}\ell \tag{3}$$

where A is the absorbance, α is the hematite absorbance coefficient (44 nm)$^{-1}$ at 400 nm [37] and ℓ is the thickness of the hematite film in nanometers. An UV–vis–NIR spectrophotometer (Shimadzu Scientific Instruments Inc., model UV-3600, Kyoto) was used to obtain the absorbance of the prepared hematite samples. It was decided to measure the reflectance and transmittance of all samples and then to calculate the absorbance by subtracting both to the incident radiation. Finally, the absorbance was corrected by subtracting the FTO glass absorbance (control).

2.5.2. Scanning electron microscopy (SEM) characterization

SEM was used to obtain information on the morphology and surface topography of the prepared materials. The morphology of the hematite films was characterized using a high-resolution scanning electron microscope (Quanta 400 FEG, FEI Company,

USA); the analyses were made at CEMUP (Centro de Materiais da Universidade do Porto). The acceleration voltage was 15 keV while an in-lens detector was employed with a working distance of about 10 mm. The surface of fresh and aged samples was examined in order to identify and analyse modifications in their surface morphology.

2.5.3. X-ray diffraction (XRD) characterization

XRD analysis was carried out in a PANalytical X'Pert MPD (Spectris plc, England) equipped with an X'Celerator detector and secondary monochromator (Cu Kα $\lambda = 0.154$ nm, 40 kV, 30 mA; data recorded at a 0.017 step size, 100 s step^{-1}). Rietveld refinement with Powder-Cell software was used to identify the crystallographic phases from the XRD diffraction patterns.

2.6. Electrolyte characterization

2.6.1. Inductively coupled plasma (ICP) technique

ICP-AES (atomic emission spectroscopy) technique was used to determine the concentration of iron in the NaOH electrolyte solution used in the stability test. Electrolyte samples of *ca.* 50 cm^3 were tested.

3. Results and discussion

3.1. Response surface methodology

A design of experiments (DoE) approach was used to optimize the bare hematite deposition. Table S2 shows the experiments plan generated by the DoE software; a second order polynomial equation was fitted to the obtained results:

$$y = a_0 + \sum_{i=1}^{3} a_i X_i + \sum_{i=1}^{3}\sum_{j=1}^{3}\left(a_{ij}X_iX_j + a_{ii}X_i^2\right) \quad (4)$$

where y is the process response, X_i are the dimensionless process factors, a_0 is the interception coefficient, a_i are the coefficients related to the dimensionless factors X_i, a_{ij} correspond to the cross interaction between different factors and a_{ii} are the coefficients related to the quadratic effects (curvature).

A standard least squares analysis was performed and the p-values ($Prob > F$) were used to assess the relevance of each factor to the process response. Smaller p-values correspond to the higher significance factors, *i.e.*, p-values < 0.05 indicate that the parameter has a relevant effect on the response with a confidence level of more than 95%. A factor has a marginal effect on the model response when $0.05 < p$-value < 0.15 and should be neglected if p-values > 0.15 [33]. Following these criteria the final model is:

$$J = 0.852 + 0.003X_1 - 0.058X_2 - 0.019X_3 + 0.016X_1X_2 + 0.053X_1X_3 - 0.066X_1^2 - 0.068X_2^2 - 0.036X_3^2 \quad (5)$$

The fitting model was used to predict the photocurrent density obtained at 1.45 V_{RHE}. Fig. 2 shows the corresponding parity plot.

The parity plot indicates a quite good agreement of the empirical model to the experimental values, which is also confirmed by the high correlation coefficient ($R^2 = 0.91$) of the fitting model. The empirical model was then used to study the influence of each operating parameter on the photocurrent density – Fig. 3. Based on the interpolating model, the operating conditions that give the highest photocurrent density at 1.45 V_{RHE}, $J = (0.90 \pm 0.06)$ mA cm^{-2}, are the following: $v = 42$ mL, $T = 425$ °C and $t = 35$ s. A new deposition was then performed using these optimal conditions and the prepared hematite samples showed an average photocurrent density of (0.94 ± 0.04) mA cm^{-2}, in line with the empirical model. The film thickness of the optimized sample, estimated from Eq. (3), was *ca.* (18.8 ± 0.1) nm; the literature refers that a film thickness of *ca.* (20.0 ± 2.2) nm maximizes the internal quantum yield [38].

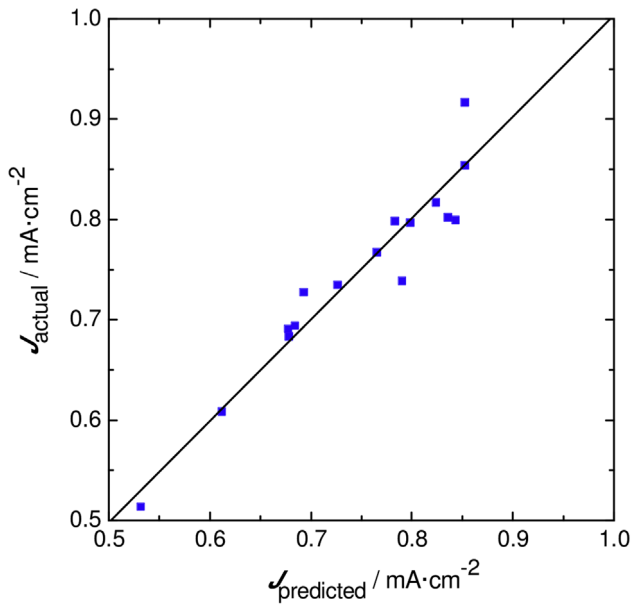

Fig. 2. Parity plot of experimental *vs.* predicted photocurrent values for the prepared hematite samples.

3.2. ***J–V characteristic curves***

The performance of the bare hematite photoanodes was assessed based on the photocurrent–voltage (J–V) curves in dark and under simulated solar illumination (AM 1.5 G, 100 mW cm^{-2}, 25 °C) conditions. The characteristic curves of each photoanode sample are summarized in Table S3 – Supplementary material. The replicated curves differ less than 10% from each other.

The J–V characteristic curve for the best performing hematite sample prepared at the optimized conditions is shown in Fig. 4a. Under dark conditions the current steeply increased for a potential higher than 1.66 V_{RHE}, indicating the electrochemical water oxidation onset potential. Under sunlight conditions the sample showed an onset potential at 0.95 V_{RHE} and photocurrent densities of *ca.* 0.67 mA cm^{-2} at the potential of reversible oxygen electrode (1.23 V_{RHE}) and *ca.* 0.94 mA cm^{-2} at 1.45 V_{RHE}. These performance values represent one of the highest photocurrents ever reported for bare hematite photoanodes. To date, the best performing hematite photoanode was reported by Tan et al. [28] for Ru-doped α-Fe_2O_3 nanorod films; however, the bare hematite sample (prepared by doctor blading method and then annealed at 750 °C) showed a low photocurrent of *ca.* 0.31 mA cm^{-2} at 1.23 V_{RHE}. Among hematite samples prepared by spray pyrolysis, the present result is *ca.* 65% greater [30].

From the J–V plots, the intrinsic power characteristics of the photoelectrode were then obtained as reported elsewhere [36]. First, the photocurrent (J_{photo}) and photopotential (V_{photo}) were determined from the difference between the light and dark currents and potentials, respectively. After computing these parameters, the J_{photo} was plotted as a function of the V_{photo} to obtain the photocurrent density measured under short-circuit conditions (J_{sc}) and the open-circuit photopotential (V_{oc}) – Fig. 4b. Consequently, the intrinsic photovoltaic power (P) of the photoanode, which is given by the product of J_{photo} by V_{photo}, was plotted versus V_{photo} (Fig. 4c). The potential applied to the photoanode under light, U_{light}, is also shown in secondary y axis of these figures *vs.* V_{photo}. Thus, the optimized hematite photoelectrode reached a

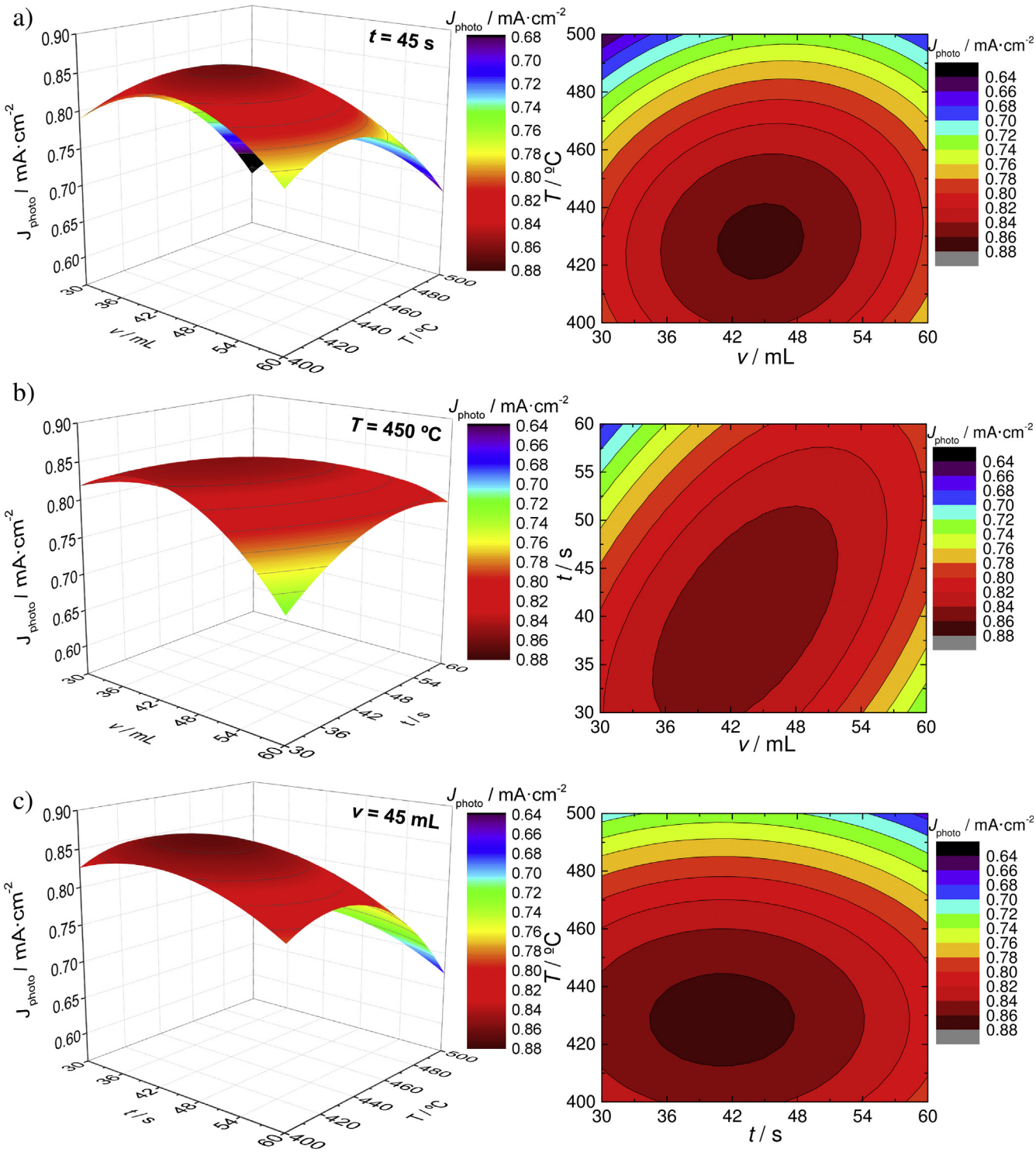

Fig. 3. Predicted photocurrent density (J) as a function of: (a) sprayed solution volume (v) and temperature of the glass substrate during the deposition (T) for a time gap between sprays of 45 s (t); (b) v and t for T=450 °C; (c) t and T for v=45 mL.

maximum power of 0.43 %, showing that this sample generated an electric power of 0.43 mW cm^{-2} from the solar-simulated light power of 100 mW cm^{-2}. At this point, the photoanode delivers the highest power with V_{MPP}=0.54 V by applying a potential, U_{light}, of *ca.* 1.30 V_{RHE}. A fill factor of 50.55% at the maximum power point was obtained; fill factor values of less than 40% are generally observed with hematite photoelectrodes [36,38].

The intrinsic solar to chemical (*ISTC*) conversion efficiency of the photoanode was computed from Eq. (2) and it was plotted in Fig. 4d as a function of the generated photocurrent density, J_{photo}. The *ISTC* efficiency reached a maximum of *ca.* 0.29% at J_{MPP} =0.80 mA cm^{-2}; this defines the optimal conditions for operating the PEC cell. This photocurrent could only be obtained in the dark at a potential of 1.85 V_{RHE} (see Fig. 4a) meaning that the simulated solar light power saved 0.54 V from the external power source, *i.e.*, a power of 0.43 mW cm^{-2} (0.54 × J_{MPP}). Therefore, the conversion efficiency of the electrolysis reaction ($\eta_{el} \approx 1.23/U_{dark}$=66.4%) reduced the electric power saved, which is the light-induced

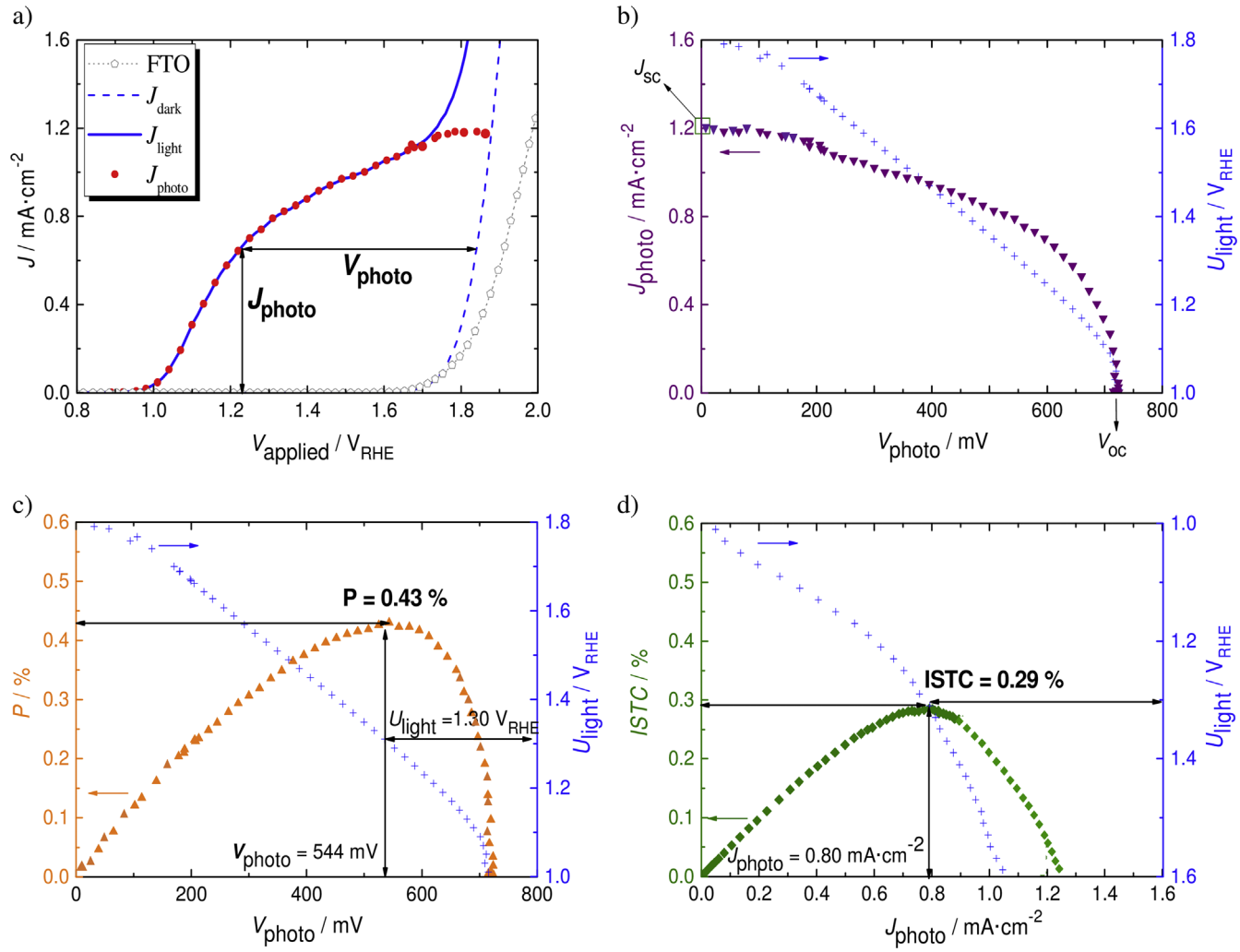

Fig. 4. (a) *J–V* characteristic curves obtained in the dark (dashed blue line) and under simulated solar illumination (AM 1.5 G, 100 mW cm^{-2}, solid blue line) and the generated photocurrent, J_{photo} (●). (b) Photocurrent (▼) as a function of the photopotential. (c) Intrinsic photovoltaic power (▲) as a function of the photopotential. (d) *ISTC* efficiency (◆) as a function of the photocurrent density. The secondary *y* axis on the right of the plots (b), (c) and (d) shows the potential (U_{light}) that was applied to the photoanode by the potentiostat, under light.

contribution to the chemical power produced by the photoanode of *ca.* 0.29 mW cm^{-2} (66.4% × 0.43 mW cm^{-2}).

3.3. Electrochemical impedance spectroscopy

The electrochemical impedance measurements were performed in the dark and using a three-electrode configuration. In this configuration the potential is measured with respect to a fixed reference potential, short-circuited with the Pt counter-electrode. This enables the detailed study of the electrochemical phenomena occurring at the interface between photoelectrode and electrolyte. Herein, the EIS data were analyzed based on the Randles electrical analog circuit [18]. This electrical analog comprises a series resistance (R_{Series}) and a simple resistor–capacitor (RC) element assigned to the semiconductor/electrolyte charge transfer resistance, R_{CT}, together with bulk capacitance, C_{Bulk} – Fig. 5a. The correspondent impedance parameters (R_{Series}, R_{CT} and C_{bulk}) are presented in Supplementary material – Fig. S1.

For using the Mott–Schottky model two main assumptions must be guaranteed: (i) the space charge (C_{SC}) and Helmholtz (C_H) capacitances can only be fitted as a single capacitance, the so-called C_{Bulk}, since the contribution of the double layer capacitance to the total capacitance would be negligible (2–3 orders of magnitude larger); and (ii) the fitting should be made at the high frequency range of the impedance spectra, in the order of kHz [37]. Then, the flat band potential, V_{FB}, and the donor density, N_D, were obtained from Eq. (6):

$$\frac{1}{C_{Bulk}^2} = \frac{2}{\varepsilon_0 \varepsilon_r q N_D A^2}\left((V_E - V_{FB}) - \frac{kT}{q} \right) \tag{6}$$

where ε_0 is the vacuum permittivity (8.85 × 10^{-12} C V^{-1} m^{-1}), ε_r is the dielectric constant of the semiconductor (assumed to be 80 for undoped hematite photoanodes [31]), q is the elementary charge, A is the active area, k is the Boltzmann constant, T is the absolute temperature, and V_E is the applied potential. Plotting C_{Bulk}^{-2} as a function of the applied bias potential, a straight line was obtained in the linear region of the plot, from 0.80 to 1.40 V_{RHE}, as shown in Fig. 5b. N_D value was determined from the slope of this line, while the V_{FB} value was obtained extrapolating the interception of the straight line with the axis of the applied potential. From Eq. (6), V_{FB}=0.54 V_{RHE} and N_D=2.42 × 10^{18} cm^{-3}. These values are in good agreement with the ones found in the literature; consistent values of V_{FB} from 0.40 to 0.60 V_{RHE} and N_D on the order of 10^{17} to 10^{21} cm^{-3} have been reported for undoped and heavily doped hematite samples, respectively [20]. Thus, the obtained value for the donor density confirmed that the pre-treatment with TEOS before spraying the ultra-thin Fe_2O_3 layer is not

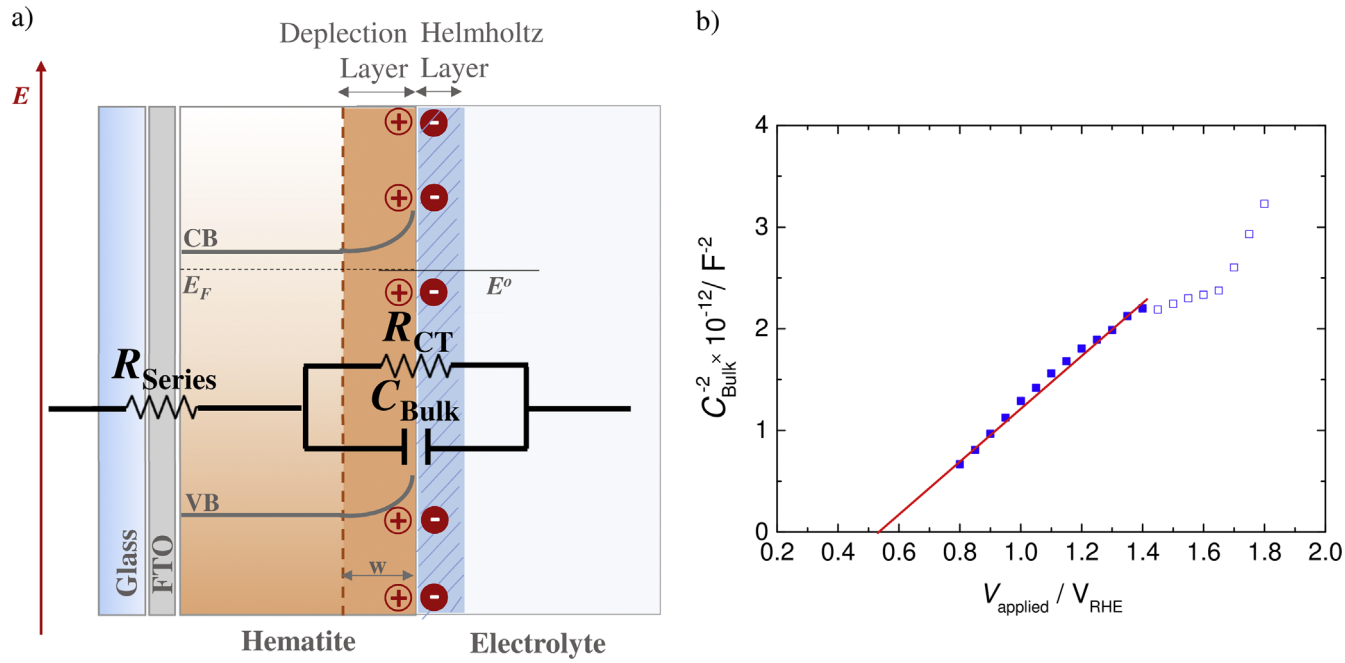

Fig. 5. (a) Energy diagram of the semiconductor/electrolyte interface and the electrical circuit analog used to fit the impedance measurements in the dark of the optimized hematite sample. (b) Mott–Schottky analysis: the inverse of the square bulk capacitance (C_{Bulk}) is plotted *vs.* the applied bias potential.

acting as a doping agent.

3.4. Long-term stability

Recent studies have increasingly mentioned the importance of obtaining highly stable photoelectrodes as a critical objective to achieve commercial viability of photoelectrochemical hydrogen production devices [39]. Therefore, the stability of the optimized hematite sample was evaluated during a period of 1000 h under a bias potential of 1.45 V_{RHE} and simulated solar illumination (100 mW cm^{-2}). The photocurrent history is plotted in Fig. 6. The photocurrent density values, obtained every 48 h, are presented in Table S4 (Supplementary material).

From Fig. 6 it can be concluded that the optimized hematite sample is stable over 1000 h (approximately 42 days) with an average photocurrent density of *ca.* 0.95 mA cm^{-2}. To the best knowledge of the authors there are no published results for stability of hematite photoanodes for such long period.

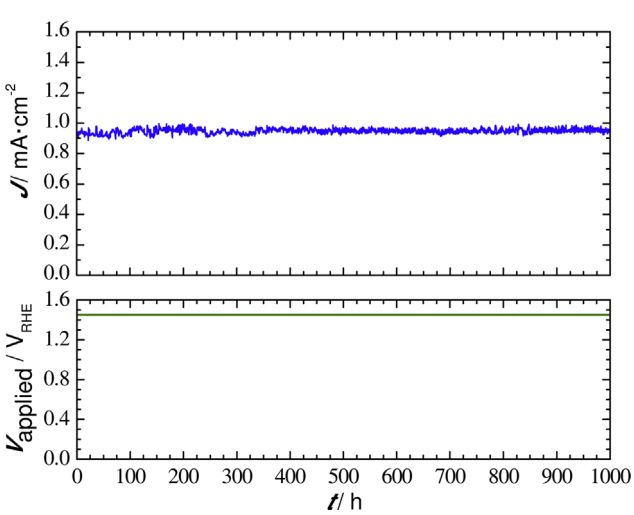

Fig. 6. Polarization curve of the optimized hematite samples prepared by spray pyrolysis (solid blue line) obtained under a constant bias of 1.45 V_{RHE} and simulated solar illumination (100 mW cm^{-2}).

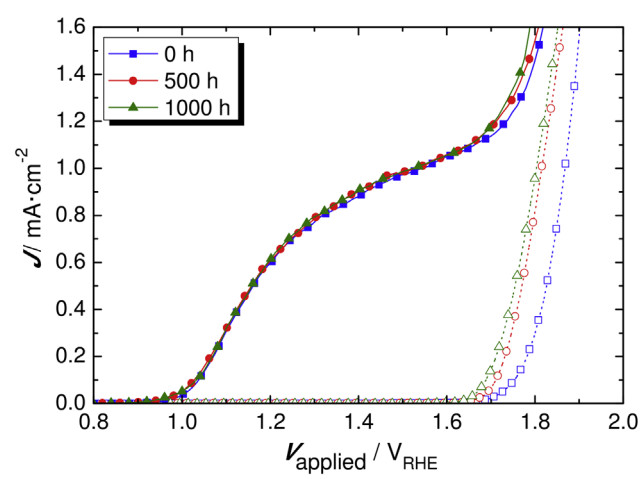

Fig. 7. *J–V* characteristics of the optimized hematite sample prepared by spray pyrolysis, before starting the stability test, 0 h (■), and after 500 h (●) and 1000 h (▲), in the dark (dashed lines) and under simulated solar illumination conditions (AM 1.5 G, 100 mW cm^{-2}, solid lines).

Fig. 7 shows the *J–V* characteristic curves obtained before performing the stability test and after 500 and 1000 h of simulated sunlight exposure; no significant differences were observed for the response under light conditions. On the other hand, the dark current onset potential shifted slightly to lower potentials, which may be related to increased FTO areas exposed to electrolyte [37,40,41]. Fig. 8 shows SEM images and EDS analyses of the fresh and aged hematite photoelectrode.

Fig. 8 confirms that the optimized hematite photoanode displays a very uniform surface fully covering the underneath FTO layer. The film growth follows a layer-plus-island growth, known as a Stranski–Krastanov mode [42,43]. The morphology is in straight agreement with previous hematite structures deposited by spray pyrolysis [44]. No significant differences are observed between the fresh and aged sample (see Fig. 8c and d, respectively). Moreover, the global EDS analyses are also similar, as

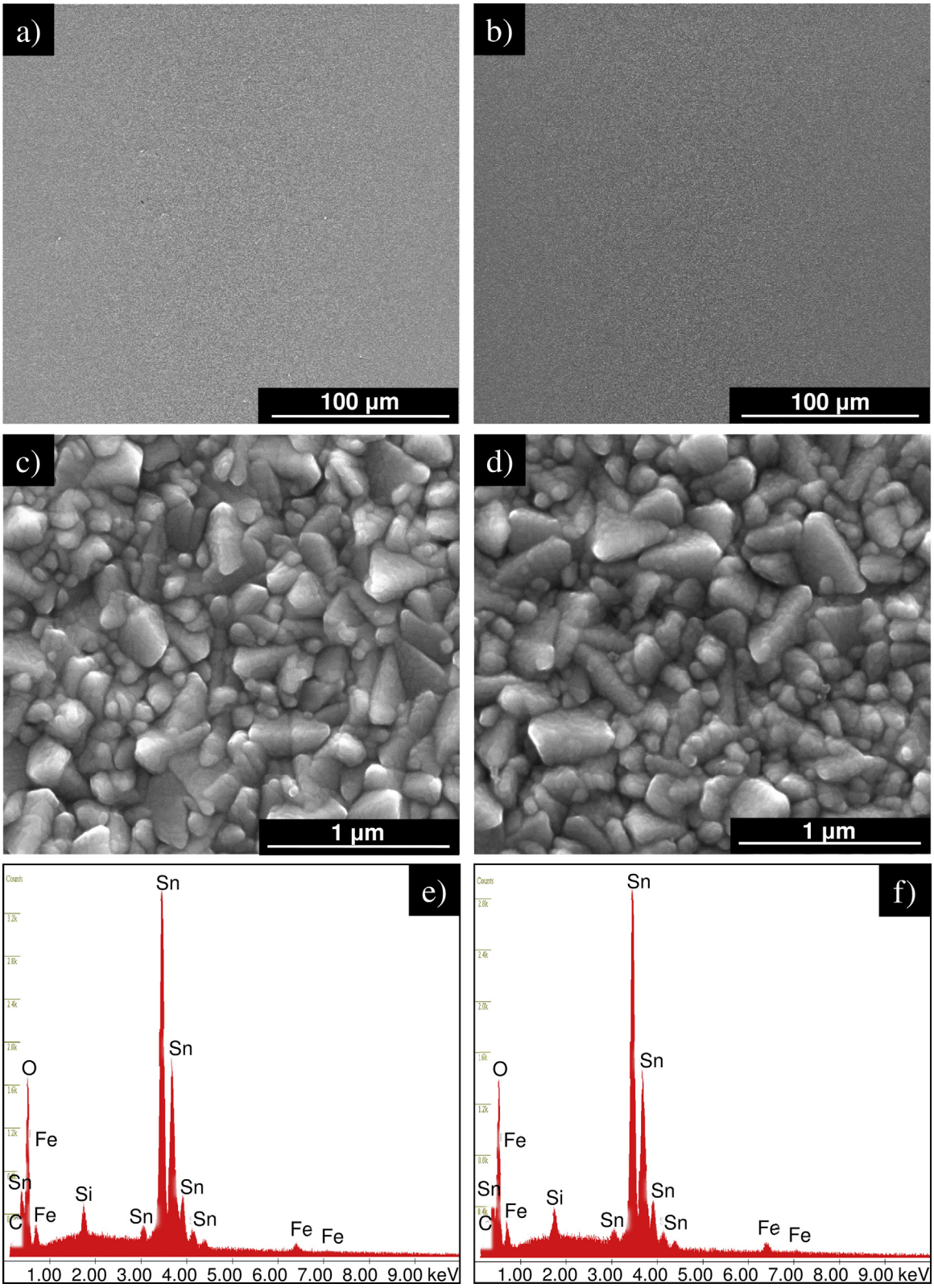

Fig. 8. Top view SEM images and EDS analyses of the optimized hematite film before [left-side] and after [right-side] the stability (1000 h).

shown in Fig. 8e and f. This behavior was not observed for hematite samples prepared using non-optimized preparation conditions. For example, a sample prepared with parameters $v=70$ mL, $T=450$ °C and $t=45$ s showed a photocurrent density of *ca.* 0.62 mA cm^{-2} at 1.45 V_{RHE}. After a stability test of 168 h the dark current onset potential increased 150 mV and the SEM images of the photoelectrode showed hematite free areas – whiter regions at Fig. S2 (Supplementary material).

X-ray diffraction (XRD) analyses (Fig. S2 – Supplementary material) of the optimized photoelectrode sample showed a very broad peak along the (110) plane found at 35.5° (reference pattern number: 01-085-0599) [24]. Since the hematite film is very thin,

ca. 19 nm, the XRD diffraction pattern should superimpose the FTO background. However, above 550 °C β-FeOOH phase originates α-Fe_2O_3 [45] and according to Kment et al. [46] highly oriented films along the (110) direction should be obtained, which facilitate electron transport in the hematite photoanodes. After the 1000 h stability period no significant changes in the film crystallinity were observed.

The electrolyte solution used in the stability test was also analyzed by inductively coupled plasma (ICP) spectroscopy; a fresh electrolyte sample was also analyzed as control. Since an iron concentration of *ca.* 88 μg L^{-1} was detected in the control, the results were merely supportive of the film corrosion hypothesis. The electrolyte used in the aging test showed an iron concentration of *ca.* 143 μg L^{-1} suggesting minimal material detachment from the film surface, probably resulting from the mechanical erosion by the oxygen evolution. Literature reports considerably high iron concentration increase during the aging tests; for example, Mendes et al. [40] reported an increase of 1 mg L^{-1} only after 72 h of aging.

4. Conclusion

The present work focused on improving the performance (photocurrent density and stability) of hematite photoanodes using a design of experiments approach. The optimized preparation parameters were: (i) amount of volume solution sprayed (v); (ii) temperature of the glass substrate during the deposition (T); and (iii) time gap between sprays (t). The set of preparation conditions found to maximize the photocurrent density were: v=42 mL, T=425 °C and t=35 s. The optimized hematite film showed a photocurrent density of *ca.* 0.94 mA cm^{-2} at 1.45 V_{RHE}, a fill factor of 50.55% and an intrinsic solar to chemical conversion efficiency of *ca.* 0.29%. SEM analysis confirmed the full surface coverage with well-organized and uniform crystals. The deposited hematite film by spray pyrolysis showed a thickness of *ca.* 18.8 nm. X-ray diffraction detected only pure α-Fe_2O_3 phase, with the (110) preferential orientation.

One of the most important contributions of this work is the long-term stability study. The prepared hematite photoanode generated a constant photoresponse over 1000 h under simulated sunlight exposure. SEM, EDS, XRD and ICP analyses confirmed the stability of the prepared hematite sample.

Acknowledgment

P. Dias and T. Lopes are grateful to FCT for their PhD and Postdoc fellows (references: SFRH/BD/62201/2009 and SFRH/BPD/102408/2014, respectively). A. Vilanova acknowledges the European Commission through the Seventh Framework Programme under Grant Agreement No. 621252 (PECDEMO). L. Andrade acknowledges the European Commission through the Seventh Framework Programme, the Specific Programme "Ideas" of the European Research Council for research and technological development as part of an Advanced Grant under Grant Agreement No. 321315 (BI-DSC). This work was financially supported by Project UID/EQU/00511/2013-LEPABE (Laboratory for Process Engineering, Environment, Biotechnology and Energy – EQU/00511) by FEDER funds through Programa Operacional Competitividade e Internacionalização – COMPETE2020 and by national funds through FCT – Fundação para a Ciência e a Tecnologia. The authors are very thankful to P. Tavares from UME-UTAD and C. Mateos-Pedrero for assisting in the interpretation of the XRD spectra and to CEMUP for the SEM and EDS analyses.

Appendix A. Supplementary material

Supplementary data associated with this article can be found in the online version at http://dx.doi.org/10.1016/j.nanoen.2016.03.008.

References

[1] EIA, Annual Energy Outlook 2015, in, U.S. Energy Information Administration, ⟨https://www.eia.gov/⟩, 2015.
[2] R. van de Krol, M. Grätzel, Introduction, in: R. van de Krol, Michael Grätzel (Eds.), Photoelectrochemical Hydrogen Production, Springer Science+Business Media, New York, USA, 2012, pp. 3–11.
[3] T. Lopes, L. Andrade, A. Mendes, Photoelectrochemical cells for hydrogen production from solar energy in solar energy sciences and engineering applications, in: A.A. Napoleon Enteria (Ed.), Solar Energy Sciences and Engineering Applications, CRC Press Taylor & Francis Group, USA, 2013, p. 692.
[4] T. Bak, J. Nowotny, M. Rekas, C.C. Sorrell, Photo-electrochemical hydrogen generation from water using solar energy. Materials-related aspects, Int. J. Hydrog. Energy 27 (2002) 991–1022.
[5] N.S. Lewis, D.G. Nocera, Powering the planet: chemical challenges in solar energy utilization, Proc. Natl. Acad. Sci. USA 103 (2006) 15729.
[6] J. Nowotny, C.C. Sorrell, L.R. Sheppard, T. Bak, Solar-hydrogen: environmentally safe fuel for the future, Int. J. Hydrog. Energy 30 (2005) 521–544.
[7] M. Grätzel, Photoelectrochemical cells, Nature 414 (2001) 338.
[8] T. Lopes, P. Dias, L. Andrade, A. Mendes, An innovative photoelectrochemical lab device for solar water splitting, Sol. Energy Mater. Sol. Cells 128 (2014) 399–410.
[9] R. Krol, Y. Liang, J. Schoonman, Solar hydrogen production with nanostructured metal oxides, J. Mater. Chem. 18 (2008) 2311–2320.
[10] T. Lopes, P. Dias, L. Andrade, A. Mendes, E-MRS/MRS bilateral energy conference innovative technological configurations of photoelectrochemical cells, Energy Procedia 22 (2012) 35–40.
[11] A. Fujishima, K. Honda, Electrochemical photolysis of water at a semiconductor electrode, Nature 238 (1972) 37–38.
[12] S.C. Warren, K. Voïtchovsky, H. Dotan, C.M. Leroy, M. Cornuz, F. Stellacci, C. Hébert, A. Rothschild, M. Grätzel, Identifying champion nanostructures for solar water-splitting, Nat. Mater. 12 (2013) 842–849.
[13] J. Liu, Y.Y. Cai, Z.F. Tian, G.S. Ruan, Y.X. Ye, C.H. Liang, G.S. Shao, Highly oriented Ge-doped hematite nanosheet arrays for photoelectrochemical water oxidation, Nano Energy 9 (2014) 282–290.
[14] L.A. Marusak, R. Messier, W.B. White, Optical absorption spectrum of hematite, α-Fe_2O_3 near IR to UV, J. Phys. Chem. Solids 41 (1980) 981–984.
[15] J.-W. Jang, C. Du, Y. Ye, Y. Lin, X. Yao, J. Thorne, E. Liu, G. McMahon, J. Zhu, A. Javey, J. Guo, D. Wang, Enabling unassisted solar water splitting by iron oxide and silicon, Nat. Commun. 6 (2015) 7447.
[16] J. Brillet, J.-H. Yum, M. Cornuz, T. Hisatomi, R. Solarska, J. Augustynski, M. Grätzel, K. Sivula, Highly efficient water splitting by a dual-absorber tandem cell, Nat. Photon. 6 (2012) 824–828.
[17] D. Gurudayal, M.H. Sabba, L.H. Kulmar, J. Wong, M. Barber, N. Mathews Grätzel, Perovskite-hematite tandem cells for efficient overall solar driven water splitting, Nano Lett. 15 (2015) 3833–3839.
[18] L. Steier, I. Herraiz-Cardona, S. Gimenez, F. Fabregat-Santiago, J. Bisquert, S. D. Tilley, M. Grätzel, Understanding the role of underlayers and overlayers in thin film hematite photoanodes, Adv. Funct. Mater. 24 (2014) 7681–7688.
[19] K.L. Hardee, A.J. Bard, Semiconductor electrodes: V. The application of chemically vapor deposited iron oxide films to photosensitized electrolysis, J. Electrochem. Soc. 123 (1976) 1024–1026.
[20] K. Sivula, F. Le Formal, M. Grätzel, Solar water splitting: progress using hematite (α-Fe_2O_3) photoelectrodes, ChemSusChem 4 (2011) 432–449.
[21] D.W. Kim, S.C. Riha, E.J. DeMarco, A.B.F. Martinson, O.K. Farha, J.T. Hupp, Greenlighting photoelectrochemical oxidation of water by iron oxide, ACS Nano 8 (2014) 12199–12207.
[22] J.W. Ager Iii, M. Shaner, K. Walczak, I.D. Sharp, S. Ardo, Experimental demonstrations of spontaneous, solar-driven photoelectrochemical water splitting, Energy Environ. Sci. 8 (2015) 2811–2824.
[23] Z. Li, W. Luo, M. Zhang, J. Feng, Z. Zou, Photoelectrochemical cells for solar hydrogen production: current state of promising photoelectrodes, methods to improve their properties, and outlook, Energy Environ. Sci. 6 (2013) 347–370.
[24] J.Y. Kim, G. Magesh, D.H. Youn, J.-W. Jang, J. Kubota, K. Domen, J.S. Lee, Single-crystalline, wormlike hematite photoanodes for efficient solar water splitting, Sci. Rep. 3 (2013) 2681.
[25] T. Hisatomi, H. Dotan, M. Stefik, K. Sivula, A. Rothschild, M. Grätzel, N. Mathews, Enhancement in the performance of ultrathin hematite photoanode for water splitting by an oxide underlayer, Adv. Mater. 24 (2012) 2699–2702.
[26] S.D. Tilley, M. Cornuz, K. Sivula, M. Grätzel, Light-induced water splitting with hematite: improved nanostructure and iridium oxide catalysis, Angew. Chem. Int. Ed. 49 (2010) 1521–13773.
[27] Q. Yu, X. Meng, T. Wang, P. Li, J. Ye, Hematite films decorated with nanostructured ferric oxyhydroxide as photoanodes for efficient and stable photoelectrochemical water splitting, Adv. Funct. Mater. 25 (2015) 2686–2692.
[28] X. Guo, L. Wang, Y. Tan, Hematite nanorods co-doped with Ru cations with

different valence states as high performance photoanodes for water splitting, Nano Energy 16 (2015) 320–328.
[29] P. Dias, M. Schreier, S.D. Tilley, J. Luo, J. Azevedo, L. Andrade, D. Bi, A. Hagfeldt, A. Mendes, M. Grätzel, M.T. Mayer, Transparent cuprous oxide photocathode enabling a stacked tandem cell for unbiased water splitting, Adv. Energy Mater. 5 (2015) 1614–6840.
[30] F. Le Formal, M. Grätzel, K. Sivula, Controlling photoactivity in ultrathin hematite films for solar water-splitting, Adv. Funct. Mater. 20 (2010) 1099–1107.
[31] I. Cesar, K. Sivula, A. Kay, R. Zboril, M. Grätzel, Influence of feature size, film thickness, and silicon doping on the performance of nanostructured hematite photoanodes for solar water splitting, J. Phys. Chem. C 113 (2008) 772–782.
[32] A. Duret, M. Gratzel, Visible light-induced water oxidation on mesoscopic α-Fe_2O_3 films made by ultrasonic spray pyrolysis, J. Phys. Chem. B 109 (2005) 17184–17191.
[33] D.C. Montgomery, Design and Analysis of Experiments, 8th ed., Wiley, New Jersey, USA, 2012.
[34] R.H. Myers, D.C. Montgomery, C.M. Anderson-Cook, Response Surface Methodology: Process and Product Optimization Using Designed Experiments, 3rd ed., Wiley, New Jersey, USA, 2011.
[35] T. Lopes, L. Andrade, H.A. Ribeiro, A. Mendes, Characterization of photoelectrochemical cells for water splitting by electrochemical impedance spectroscopy, Int. J. Hydrog. Energy 35 (2010) 11601–11608.
[36] H. Dotan, N. Mathews, T. Hisatomi, M. Grätzel, A. Rothschild, On the solar to hydrogen conversion efficiency of photoelectrodes for water splitting, J. Phys. Chem. Lett. 5 (2014) 3330–3334.
[37] T. Lopes, L. Andrade, F. Le Formal, M. Grätzel, K. Sivula, A. Mendes, Hematite photoelectrodes for water splitting: evaluation of the role of film thickness by impedance spectroscopy, Phys. Chem. Chem. Phys. 16 (2014) 16515–16523.
[38] B.M. Klahr, T.W. Hamann, Current and voltage limiting processes in thin film hematite electrodes, J. Phys. Chem. C 115 (2011) 8393–8399.
[39] T.J. Jacobsson, V. Fjallstrom, M. Edoff, T. Edvinsson, Sustainable solar hydrogen production: from photoelectrochemical cells to PV-electrolyzers and back again, Energy Environ. Sci. 7 (2014) 2056–2070.
[40] P. Dias, T. Lopes, L. Andrade, A. Mendes, Temperature effect on water splitting using a Si-doped hematite photoanode, J. Power Sources 272 (2014) 567–580.
[41] P. Dias, T. Lopes, L. Meda, L. Andrade, A. Mendes, Photoelectrochemical water splitting using WO_3 photoanodes: the substrate and temperature roles, Phys. Chem. Chem. Phys. 18 (2016) 5232–5243.
[42] D.J. Eaglesham, M. Cerullo, Dislocation-free Stranski–Krastanov growth of Ge on Si(100), Phys. Rev. Lett. 64 (1990) 1943–1946.
[43] F. Le Formal, M. Grätzel, K. Sivula, Controlling photoactivity in ultrathin hematite films for solar water-splitting, Adv. Funct. Mater. 20 (2010) 1099–1107.
[44] F. Le Formal, N. Tetreault, M. Cornuz, T. Moehl, M. Grätzel, K. Sivula, Passivating surface states on water splitting hematite photoanodes with alumina overlayers, Chem. Sci. 2 (2011) 737–743.
[45] A. Annamalai, A. Subramanian, U. Kang, H. Park, S.H. Choi, J.S. Jang, Activation of hematite photoanodes for solar water splitting: effect of FTO deformation, J. Phys. Chem. C 119 (2015) 3810–3817.
[46] S. Kment, P. Schmuki, Z. Hubicka, L. Machala, R. Kirchgeorg, N. Liu, L. Wang, K. Lee, J. Olejnicek, M. Cada, I. Gregora, R. Zboril, Photoanodes with fully controllable texture: the enhanced water splitting efficiency of thin hematite films exhibiting solely (110) crystal orientation, ACS Nano 9 (2015) 7113–7123.

Paula Dias received the MSc degree in chemical engineering from the Faculty of Engineering, University of Porto, Portugal, in 2010. She is currently doing the PhD degree in photoelectrochemical (PEC) cells for solar energy conversion and storage at Laboratory for Process Engineering, Environment, Biotechnology and Energy (LEPABE). Her research interests include development of efficient and stable photoelectrodes and innovative tandem devices for unbiased solar water splitting.

António Vilanova obtained a MSc degree in environmental engineering from University of Porto in 2014. Currently, works as a PhD student at the same institution. His research activities are focused on photoelectrochemical cells for solar energy conversion and storage; preparation of efficient materials for solar hydrogen production. Research areas of special interest include the design, optimization and CFD modelling of photoelectrochemical prototypes for industrial applications.

Tânia Lopes obtained a PhD in chemical and biological engineering from University of Porto in 2014. Currently, works as a postdoc researcher at the same institution. Her research activities are focused on photoelectrochemical cells for solar energy conversion and storage; experimental and theoretical studies under steady-state and time-resolved methods. Special interest is being given to the development of innovative photoelectrochemical device prototypes engineered to foster industrial applications.

Luísa Andrade received her PhD degree from the University of Porto in 2010 with the thesis entitled "Study and Characterization of Grätzel Solar Cells". She is currently senior researcher at University of Porto. Develops research activities in photovoltaic cells (perovskite and Grätzel cells), photoelectrochemical cells for the production of solar hydrogen and photocatalysis. Her publications include more than 25 research papers in peer-reviewed scientific journals, 3 book chapters; she is co-author of 8 patents. She is researcher in 9 projects (5 national and 4 international). She was awarded with ACP Diogo Vasconcelos (2011), Solvay & Hovione Innovation Challenge 2011 (SHIC'11) and Ramos Catarino (2011–2012) prizes.

Adélio Mendes is full professor at FEUP and researcher at LEPABE, where he leads the Energy, Processes and Products area. His publications include over 250 papers in peer-reviewed scientific journals and 5 reviews or invited book chapters. He is the inventor or co-inventor of over 20 patents and authored one book. Prof. Mendes is presently the coordinator of project BeingEnergy (Grant agreement no: 303476), project BI-DSC (advanced research grant from ERC) and GOTSolar (Grant agreement no: 687008). He was awarded with Air Products Faculty Excellence Award (2011), ACP Diogo Vasconcelos (2011) and Solvay & Hovione Innovation Challenge 2011 (SHIC'11) prizes.